JHEP

Published by Institute of Physics Publishing for SISSA

Received: *December 26, 2006*
Accepted: *February 13, 2007*
Published: *March 5, 2007*

Chiral crystals in strong-coupling lattice QCD at nonzero chemical potential

Barak Bringoltz

Rudolf Peierls Centre for Theoretical Physics, University of Oxford,
1 Keble Road, Oxford, OX1 3NP, U.K.
E-mail: barak@thphys.ox.ac.uk

Abstract: We study the effective action for strong-coupling lattice QCD with one-component staggered fermions in the case of nonzero chemical potential and zero temperature. The structure of this action suggests that at large chemical potentials its ground state is a crystalline 'chiral density wave' that spontaneously breaks chiral symmetry and translation invariance. In mean-field theory, on the other hand, we find that this state is unstable. We show that lattice artifacts are partly responsible for this, and suggest that if this phase exists in QCD, then finding it in Monte-Carlo simulations would require simulating on relatively fine lattices. In particular, the baryon mass in lattice units, m_B, should be considerably smaller than its strong-coupling limit of $m_B \sim 3$.

Keywords: Strong Coupling Expansion, Lattice QCD, Spontaneous Symmetry Breaking, Lattice Quantum Field Theory.

JHEP03(2007)016

Contents

1. Introduction

The idea that the ground state of QCD at zero temperature and nonzero chemical potential can spontaneously break translation invariance was first suggested by Deryagin, Grigoriev and Rubakov (DRG) [1]. They studied large-N QCD at weak coupling, and showed that the four-quark interaction, that is generated by a single gluon exchange, causes an instability in the quark Fermi sea toward the creation of a condensate of the form

$$\langle \bar{\psi}(x)\psi(x)\rangle \sim \cos\left(2\vec{Q}\cdot\vec{x}\right). \tag{1.1}$$

Here the wave vector $\vec{Q}$ has an arbitrary direction but its modulus is given by the Fermi momentum of the quarks

$$Q = p_F. \tag{1.2}$$

This phenomenon is often referred to as chiral density waves, and has famous solid-state counterparts like the one-dimensional Peierls instability [2], and the spin density wave of the Overhauser effect [3].

The large-N result of [1] was consequently found to be misleading [4, 5], and Shuster and Son showed in [4] that if N is decreased from infinity to $N \lesssim O(1000)$, then color-superconductivity becomes preferable over the DGR state. Nonetheless, the authors in [6] studied what may happen at lower densities (for $N = 3$), where weak coupling treatments are less reliable [7]. The conclusion of [6] was that chiral density waves may still be competitive with superconductivity, especially when one uses an instanton vertex to couple the quarks.

Recently, there has been related progress in the Gross-Neveu model. This $1+1$ model can be studied in large-N, and its phase structure in the temperature-density plane was known to have a line of first order transitions that separate a low density phase with spontaneously broken chiral symmetry, and a high density phase, where this symmetry is intact. This structure arises when one restricts to an x-independent ansatz for $\langle\bar{\psi}(x)\psi(x)\rangle$ and was recently revisited in [8] (and later with a lattice regularisation in [9]), where the condensate was allowed to depend on the spatial coordinate of x. The study in [8] discovered a new phase at low temperatures and high densities, which is separated by a second order phase transition from the low density phase, and where the chiral condensate has a crystalline structure. This crystal structure was also seen in the 't Hooft model [10], and is reminiscent of results from older work in the Skyrme model [11].

In this paper we look for a phase with chiral density waves using an effective action that is derived from the strong-coupling expansion of lattice QCD. Apart from a phenomenological interest in this model, and in the way it may expose the phase we are after, we are also motivated by the following, more practical, reason. Future Monte-Carlo simulations of QCD at low temperatures and large chemical potentials, that will manage to control the sign problem, will presumably start by simulating relatively coarse lattices with strong couplings. This makes the knowledge on the phase diagram of the strong-coupling limit important, and in our context it is desirable to know whether one should expect a crystal phase, and if so, at which values of the chemical potential μ.

Indeed, numerous authors have analytically investigated the phase diagram of the strong-coupling limit (for reviews see [12, 13]), but the possibility to have chiral density waves was never considered, and these works were always restricted to homogeneous field configurations.

Here we relax this constraint for the first time. To do so, we choose to work with one-component staggered fermions. In four dimensions, these lattice fermions describe four degenerate continuum Dirac fermions, commonly referred to as tastes. The continuum theory has an $\mathrm{SU}(4) \times \mathrm{SU}(4)$ chiral symmetry, that explicitly breaks on the lattice to the following axial taste non-singlet $\mathrm{U}(1)$

$$\begin{aligned} \psi &\to \exp\left(i\theta\,\gamma_5 \otimes \xi_5\right)\,\psi, \\ \bar{\psi} &\to \bar{\psi}\,\exp\left(i\theta\,\gamma_5 \otimes \xi_5\right). \end{aligned} \tag{1.3}$$

Here ξ_5 is a 4×4 traceless matrix that operates in taste space, and that can be chosen to have the same matrix elements of γ_5. The ground state that we study in this paper is

characterised by the helical condensates

$$\langle \bar{\psi}(x)\, \psi(x) \rangle \sim \cos\left(2\vec{Q}\cdot\vec{x}\right), \tag{1.4}$$

$$\langle \bar{\psi}(x)\, (i\,\gamma_5 \otimes \xi_5)\, \psi(x) \rangle \sim \sin\left(2\vec{Q}\cdot\vec{x}\right), \tag{1.5}$$

that spontaneously break the chiral symmetry of eq. (1.4) as well as translation invariance. Note that eqs. (1.4)–(1.5) cannot be rotated by a global transformation to have $\langle \bar{\psi}(x)\, (\gamma_5 \otimes \xi_5)\, \psi(x) \rangle = 0$. This means that if we regard the continuum limit as a theory of four degenerate light quarks, then our chiral waves break SU(4) flavor. As a result, we are studying a ground state which is closer to the one studied in [14] than to the original DGR state, which is a flavor singlet.

The reason we choose this particular type of lattice fermions is that, in the strong-coupling limit, they give rise to a very simple effective action in terms of hadrons. This action was derived some time ago by Hoek, Kawamoto, and Smit [15], and in the next section we re-derive it for self-completeness. After discussing why it is natural to expect chiral density waves in the ground state of this action (at nonzero μ), we formulate in section 3 a mean-field theory that is general enough to allow for such chiral waves to emerge. The mean-field equations are solved in section 4, where we also investigate how the mean-field ground state evolves when we increase μ. We conclude in section 5 with a few remarks on the implications of this work and on future prospects. Appendix A includes technical details related to the calculation of the mean-field equations and the mean-field free energy.

2. The effective action

In this section we follow the work of Hoek, Kawamoto, and Smit (HKS) [15], and re-derive their effective action. Readers who are familiar with [15] can proceed to section 2.2, where we discuss the structure of the effective action, and why it is natural to expect a chiral density wave in its ground state at nonzero μ.

2.1 Deriving the Hoek-Kawamoto-Smit action for hadrons

The starting point is the strong-coupling limit of an SU(N) lattice gauge theory with one-component staggered fermions. The action in this case is

$$S = -\frac{1}{2}\sum_{n,\nu}\left[\bar{\chi}_n \eta_{n\nu} U_{n\nu} \chi_{n+\hat{\nu}} - \bar{\chi}_{n+\hat{\nu}} \eta_{n\nu}^{-1} U_{n\nu}^{\dagger} \chi_n\right] + \sum_n \left[N J_n M_n + \bar{c}_n B_n + \bar{B}_n c_n\right], \tag{2.1}$$

where $n = (n_0, n_1, \ldots, n_d)$ is an Euclidean lattice index and $\nu = 0, 1, 2, \ldots, d$ is the direction index (d is the number of spatial dimensions). The fields χ and $\bar{\chi}$ are independent Grassmann variables and $U_{n\nu}$ is an SU(N) matrix that represents the gauge fields. The factors $\eta_{n\nu}$ are the Kogut-Susskind factors that give the fermions their Dirac structure

$$\eta_{n\nu} = \begin{cases} e^{\mu} & \nu = 0, \\ (-1)^{n_0 + n_1 + \ldots + n_{\nu-1}} & \nu \in [1, d], \end{cases} \tag{2.2}$$

and here $\mu \geq 0$ is the quark chemical potential in units of the lattice spacing [16]. The source terms J, c, and $\bar{c}$ couple to the following meson and baryon fields

$$\begin{aligned} M_n &= \frac{1}{N}\sum_{a=1}^{N} \chi_{n,a}\bar{\chi}_{n,a}, \\ B_n &= \chi_{n,1}\chi_{n,2}\cdots\chi_{n,N}, \\ \bar{B}_n &= \bar{\chi}_{n,N}\bar{\chi}_{n,N-1}\cdots\bar{\chi}_{n,1}, \end{aligned} \tag{2.3}$$

and as indicated here, the only internal index that χ_n and $\bar{\chi}_n$ carry, is the color index $a = 1, \ldots, N$. This leads to significant simplifications compared to the flavoured case, because it means that $(M_n)^k = 0$ for $k > N$, and $(B_n)^k = (\bar{B}_n)^k = 0$ for $k > 1$ [17, 15].

Since the plaquette term is absent in eq. (2.1), one can readily integrate over the SU(N) link matrices. This is performed link by link and the result is

$$\begin{aligned} Z(J,c,\bar{c}) &= \int D\bar{\chi}\, D\chi\, DU \exp S = \int D\bar{\chi}\, D\chi\, \exp S_1(M,B,\bar{B}), \\ S_1 &= \sum_{n\nu}\left\{ NF_N(M_nM_{n+\hat{\nu}}) - \frac{2^{-N+1}}{2}\left[\bar{B}_n\left(\eta_{n\nu}\right)^N B_{n+\hat{\nu}} - \bar{B}_{n+\hat{\nu}}\left(\eta_{n\nu}\right)^{-N} B_n\right]\right\} \\ &\quad + \sum_n \left\{ NJ_nM_n + \bar{c}_nB_n + \bar{B}_nc_n\right\}. \end{aligned} \tag{2.4}$$

Here the function F_N is known for several values of N [18], and in particular, for SU(3), it is

$$F_3(u) = \frac{1}{4}u + \frac{3}{64}u^2 - \frac{15}{256}u^3. \tag{2.5}$$

The next step is to write Z as a path integral over *color-singlet* fields. This is accomplished by first writing

$$Z = \exp\left[S_1(\frac{1}{N}\partial_J, -\partial_c, \partial_{\bar{c}})\right] Z_0, \tag{2.6}$$

$$Z_0 = \int D\bar{\chi}D\chi \exp\left\{\sum_n \left[NJ_nM_n + \bar{B}_nc_n + \bar{c}_nB_n\right]\right\}. \tag{2.7}$$

Performing the integral over χ and $\bar{\chi}$ results in (here we assume that N is odd)

$$Z_0 = \prod_n \left[J_n^N + \bar{c}_nc_n\right], \tag{2.8}$$

that can be written as

$$Z_0 = \int D\bar{b}\, Db\, Dm\, \exp\left\{\sum_n \left[-d_N\bar{b}_nm_n^{-N}b_n + NJ_nm_n + \bar{c}_nb_n + \bar{b}_nc_n\right]\right\}, \tag{2.9}$$

with $d_N = N!/N^N$. Here b_n and $\bar{b}_n$ are Grassmann variables, and the field $m_n = e^{i\theta_n}$ takes values on the unit circle and has the measure

$$\int dm_n \equiv \oint \frac{dm_n}{2\pi i m_n} = \int_{-\pi}^{\pi} \frac{d\theta_n}{2\pi}. \tag{2.10}$$

We are now ready to apply eq. (2.6) and doing so one obtains (setting $J = c = \bar{c} = 0$, and replacing $b \to -2^{N-1}b$)

$$Z = \int D\bar{b}\, Db\, Dm\, \exp(S_{\rm HKS}), \tag{2.11}$$

$$S_{\rm HKS} = S_{\rm Meson} + S_{\rm Baryon} + S_I, \tag{2.12}$$

$$S_{\rm Meson} = \sum_{n\nu} N F_N(m_n m_{n+\hat{\nu}}), \tag{2.13}$$

$$S_{\rm Baryon} = \sum_{nm} \bar{b}_n\, D_{nm}\, b_m, \tag{2.14}$$

$$S_I = \sum_{n} \bar{b}_n b_n\, \left(2^{N-1} d_N m_n^{-N}\right). \tag{2.15}$$

Here D is the massless Dirac operator of a free one-component staggered fermion whose chemical potential is equal to $N\mu$,

$$D_{n,m} = \frac{1}{2}\left\{\left[\delta_{m,n+\hat{0}} e^{N\mu} - \delta_{m,n-\hat{0}} e^{-N\mu}\right] + \sum_{\nu=1}^{d} \eta_{n\nu}\left[\delta_{m,n+\hat{\nu}} - \delta_{m,n-\hat{\nu}}\right]\right\}. \tag{2.16}$$

Since the composite fields M_n, B_n, and $\bar{B}_n$ in eq. (2.1) couple to the same currents as m_n, b_n, and $\bar{b}_n$ of $S_{\rm HKS}$ (see eq. (2.9)), then their correlation functions are the same. This means that the fields b_n and m_n represent the baryons and mesons respectively. Their hopping on the lattice is described by $S_{\rm Baryon}$ and $S_{\rm Meson}$, while the latter also describes meson-meson interactions. Interactions between mesons and baryons are described by the Yukawa-like vertex S_I, which in terms of quarks, represents a rearrangement of N quark-antiquark pairs into a single baryon-antibaryon pair.

2.2 Chiral density waves from $S_{\rm HKS}$?

The purpose of this section it is to show why it is natural to expect that chiral density waves emerge from $S_{\rm HKS}$ (eq. (2.12)). We begin with section 2.2.1 by formulating the chiral wave ansatz of eqs. (1.4)–(1.5) in terms of the fields that appear in $S_{\rm HKS}$, and proceed to section 2.2.2, where we explain the mechanism by which these waves can arise.

2.2.1 The chiral density wave ansatz with staggered fermions

We begin with constructing the condensates in eqs. (1.4)–(1.5). To do so we define a new lattice with spacing $a = 2$ that has 2^{d+1} sites in its unit cell (This is the lattice of hypercubes used to define the taste basis [19]). The original lattice coordinate n is related to the new one X by

$$n = 2X + \rho, \tag{2.17}$$

where the $(d+1)$-dimensional vector ρ has $\rho_\nu = 0, 1$, and denotes the internal sites in the unit cell. The mean-field ansatz that we study in this paper is

$$\langle \left(\frac{\bar{\chi}_n \chi_n}{N}\right)^q \rangle = \langle\, (m_n)^q \,\rangle = V_q\; e^{iq\,\vec{Q}\,\vec{n}\,\epsilon_n}, \qquad q = 1, 2, \ldots, N. \tag{2.18}$$

where the sign factor ϵ_n is given by

$$\epsilon_n = (-1)^{\sum_{\nu=0}^{d} n_\nu} = \begin{cases} +1 & \text{even site} \\ -1 & \text{odd site} \end{cases} \tag{2.19}$$

The appearance of this sign factor in the phases of the condensates realises the helical structure of eqs. (1.4)–(1.5) in the staggered formalism. To see this, we transform to taste basis with the unitary transformation U [19]

$$\chi_\rho(X) \equiv \sum_{\alpha=1}^{2^{D/2}} \sum_{f=1}^{2^{D/2}} \left(U^\dagger\right)_{\rho,(\alpha,f)} \psi_{\alpha,f}(X), \tag{2.20}$$

$$\bar{\chi}_\rho(X) \equiv \sum_{\alpha=1}^{2^{D/2}} \sum_{f=1}^{2^{D/2}} \bar{\psi}_{\alpha,f}(X) U_{(\alpha,f),\rho}, \tag{2.21}$$

$$U_{(\alpha,f),\rho} = \mathcal{N}_0 \left(\prod_{\nu=1}^{D} \gamma_\nu^{\rho_\nu} \right)_{\alpha,f}. \tag{2.22}$$

Here $D = d + 1$ is the number of spacetime dimensions, which we restrict to $D = 1 + 1$ or $D = 3 + 1$. The indices α and f are identified with the Dirac and taste indices respectively, and (α, f) is a composite index that takes 2^D values. The normalisation $\mathcal{N}_0$ is chosen to have $U^\dagger U = \mathbf{1}$, and the matrices γ_μ are the Euclidean Dirac matrices.[1] Using eqs. (2.20)–(2.22) and the fact that the sign factor ϵ_n depends only on ρ,

$$\epsilon_n = \epsilon_{2X+\rho} = (-1)^{\sum_\nu \rho_\nu} \equiv \epsilon_\rho, \tag{2.23}$$

we can write

$$\sum_\rho \langle \bar{\chi}_\rho(X) \chi_\rho(X) \rangle = \sum_{\alpha,f} \langle \bar{\psi}_{\alpha,f}(X) \psi_{\alpha,f}(X) \rangle \equiv \langle \bar{\psi}(X) \psi(X) \rangle, \tag{2.24}$$

$$\begin{aligned} \sum_\rho \langle \bar{\chi}_\rho(X)\, i\epsilon_\rho\, \chi_\rho(X) \rangle &= i \sum_{\substack{\alpha,f \\ \alpha',f'}} \langle \bar{\psi}_{\alpha,f}(X)\, (\gamma_5)_{\alpha\alpha'}\, (\xi_5)_{ff'}\, \psi_{\alpha',f'}(X) \rangle \\ &\equiv \langle \bar{\psi}(X)\, i\, (\gamma_5 \otimes \xi_5)\, \psi(X) \rangle. \end{aligned} \tag{2.25}$$

Here γ_5 and ξ_5 have the same matrix elements, and act in Dirac and taste space respectively. Substituting eq. (2.18) in the left hand side of eqs. (2.24)–(2.25) and using eq. (2.23) gives

$$\langle \bar{\psi}(X)\, \psi(X) \rangle = A \cos\left(2\vec{Q} \cdot \vec{X} + \phi\right), \tag{2.26}$$

$$\langle \bar{\psi}(X)\, (i\gamma_5 \otimes \xi_5)\, \psi(X) \rangle = -A \sin\left(2\vec{Q} \cdot \vec{X} + \phi\right), \tag{2.27}$$

with

$$\phi \equiv \frac{1}{2} \sum_{\nu=1}^{d} Q_\nu, \tag{2.28}$$

$$A \equiv 2V_1 \begin{cases} \cos\left(\frac{1}{2}Q_1\right) & d = 1 \\ \cos\phi + \sum_{\nu=1}^{3} \cos\left(\frac{1}{2}Q_\nu - \frac{1}{2}\sum_{\mu\neq\nu} Q_\nu\right) & d = 3 \end{cases}, \tag{2.29}$$

[1] In $d = 1$ we choose $(\gamma_0, \gamma_1, \gamma_5)$ to be the Pauli matrices $(\sigma_z, \sigma_y, \sigma_x)$, and in $d = 3$ we use the convention of [19].

By performing the chiral rotation of eq. (1.4) with $\theta = \phi/2$ we get rid of the angle ϕ in the arguments of the sine and cosine functions in eqs. (2.26)–(2.27), and obtain the assured helical structure of eqs. (1.4)–(1.5).

2.2.2 The mechanism of the chiral density wave instability

We now proceed to show that the Yukawa-like interaction, S_I, can make the state characterised by eq. (2.18) become the ground state of $S_{\rm HKS}$ (eq. (2.12)) at $\mu > 0$. For simplicity, we consider the $d = 1$ case only.

In the absence of S_I, the baryons behave like free massless fermions, and it is straightforward to show that the poles of the propagator D^{-1} of eq. (2.14) are determined in momentum space by

$$0 = \left[\sin^2(p_0/2 - i\mu N) + \sin^2(p_1/2)\right]^2 \quad ; \quad -\pi \leq p_{0,1} \leq +\pi. \tag{2.30}$$

eq. (2.30) tells us that $S_{\rm Baryon}$ describes the four energy bands

$$\sinh E_0^{(1),(2)}(p_1) = +|\sin(p_1/2)|, \tag{2.31}$$
$$\sinh E_0^{(3),(4)}(p_1) = -|\sin(p_1/2)|, \tag{2.32}$$

with $p_1 \in [-\pi, +\pi]$, and that the Fermi energy and Fermi momentum of the baryons are

$$E_F = \mu N, \tag{2.33}$$
$$\sin p_F/2 = \sinh N\mu. \tag{2.34}$$

To take $S_I(b, \bar{b}, m)$ into account we use mean-field theory, and replace the meson fields by their condensates. In the next section we find that with the mean-field ansatz of eq. (2.18) we should replace S_I with

$$S_I^{\rm mean-field} \equiv \sum_n \bar{b}_n b_n \left(\Sigma\, e^{-iNQ\, n_1\, \epsilon_n}\right), \tag{2.35}$$

where the amplitude Σ is a complicated function of the amplitudes $V_{1,2,\ldots,N}$ from eq. (2.18). In terms of the lattice coordinates of the new lattice eq. (2.35) becomes

$$S_I^{\rm mean-field} = \sum_{X\rho} \bar{b}_\rho(X) b_\rho(X) \left(\Sigma e^{-iN\,Q\,(2X_1+\rho_1)\,\epsilon_\rho}\right), \tag{2.36}$$

where we defined $b_n = b_{2X+\rho} \equiv b_\rho(X)$ and similarly for $\bar{b}$.

Clearly, $S_I^{\rm mean-field}$ mixes baryons whose momenta differ by the amount $\delta p_1 = 2NQ$. The strongest effect will occur between baryons that in the absence of S_I are degenerate in energy, and in particular, this mixing can occur between the bands $E^{(1)}$ and $E^{(2)}$ of eq. (2.31). This will lead to level repulsion, and to the opening of a gap in the spectrum.

To see this explicitly we move to momentum space with[2]

$$b_\rho(X) = \sqrt{\frac{4}{N_s}}\, e^{-i\epsilon_\rho NQ(2X_1+\rho_1)/2} \sum_p e^{+ipX}\, b_\rho(p), \tag{2.37}$$

$$\bar{b}_\rho(X) = \sqrt{\frac{4}{N_s}}\, e^{-i\epsilon_\rho NQ(2X_1+\rho_1)/2} \sum_p e^{-ipX}\, \bar{b}_\rho(p). \tag{2.38}$$

Note that eqs. (2.37)–(2.38) are not a usual Fourier transform, because they gives the field $b_\rho(p)$ a momentum that differs from the momentum of $\bar{b}_\rho(p)$ by an amount $\delta p_1 = 2NQ\epsilon_\rho$. This makes $S_I^{\rm mean-field}$ diagonal in p space, and we find that the contributions of the baryons to $S_{\rm HKS}$ are given by

$$S_{\rm Baryon} + S_I^{\rm mean-field} \equiv \sum_{\substack{p\\ \rho\rho'}} \bar{b}_\rho(p)\, K_{\rho\rho'}(p)\, b_{\rho'}(p), \tag{2.39}$$

where the Dirac operator K is

$$K_{\rho\rho'}(p) = \left[\Gamma_0 \sin\left(p_0/2 - i\mu N\right) + \Gamma_1 \sin\left(p_1/2 + \hat{\epsilon}\, QN/2\right) + \Sigma\, \mathbf{1}\right]_{\rho\rho'}. \tag{2.40}$$

Here

$$(\hat{\epsilon})_{\rho\rho'} \equiv \epsilon_\rho \delta_{\rho\rho'}, \tag{2.41}$$

$$(\Gamma_\nu)_{\rho\rho'} \equiv \tilde{\eta}_\nu \left(\delta_{\rho',\rho+\hat{\nu}} + \delta_{\rho',\rho-\hat{\nu}}\right) e^{ip(\rho-\rho')/2}, \tag{2.42}$$

with $\tilde{\eta}_0 = 1$ and $\tilde{\eta}_1 = (-1)^{\rho_0}$. Using the methods of appendix A, it is easy to calculate the determinant of $K(p)$, extract its roots, and find that the four energy levels in eqs. (2.31)–(2.32) are modified to two positive energies,

$$\sinh E_\pm = + \left| \sqrt{\Sigma^2 + \left(\sin(p_1/2)\cos(NQ/2)\right)^2} \pm \cos(p_1/2)\sin(NQ/2) \right|, \tag{2.43}$$

and two negative energies $\bar{E}_\pm = -E_\pm$. We plot $E_\pm$ in figure 1, where we choose $\Sigma = Q = 0$ (black solid lines), $\Sigma = 0.1$ and $NQ = \pi/4$ (dashed blue lines), and $\Sigma = 0.1$ and $Q = 0$ (dotted green lines). Note that the case with $\Sigma = 0$ corresponds to the absence of S_I and the band structure should not depend on Q. Indeed, from eq. (2.43) we see that if $\Sigma = 0$ the energies $E_\pm$ reduce to $E^{(1),(2)}$ (up to a shift of $\pm NQ$ from the origin, that can be removed by redefining the Brillouin Zone).

Next, consider the following choice of the wave-vector Q

$$NQ = p_F. \tag{2.44}$$

Together with eq. (2.34) and eq. (2.31), this identifies the dashed-dotted horizontal line of figure 1 with the Fermi level eq. (2.33), in which case the effect of the level repulsion is to

[2]Although we insert identical phases of $\epsilon_\rho NQ(2X_1+\rho_1)/2$ into eq. (2.37) and eq. (2.38), the transform between X-space and p-space still has a unit determinant due to the sign factor ϵ_ρ. (On a lattice with an even number of sites in each direction).

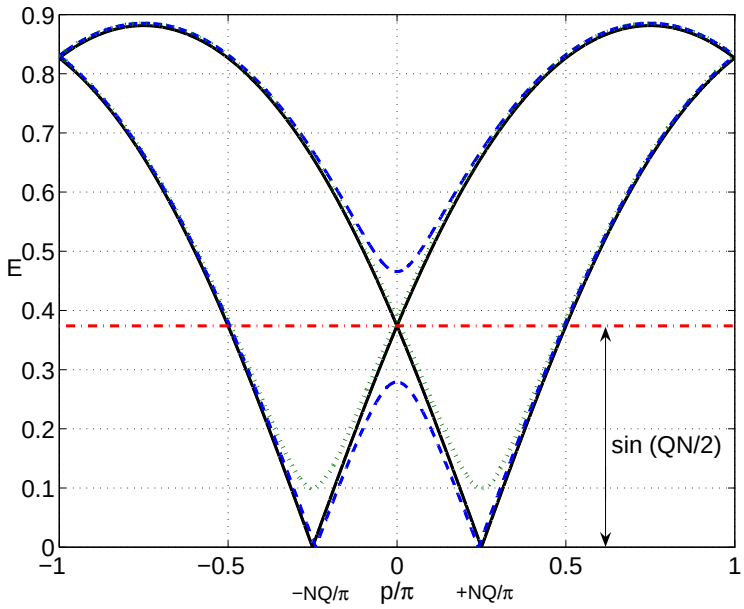

Figure 1: Dispersion relations $E_\pm$: $\Sigma = Q = 0$ (black solid lines), $\Sigma = 0.1$ and $NQ = \pi/4$ (dashed blue lines), and $\Sigma = 0.1$, and $Q = 0$ (dotted green lines). Note that the solid and dotted lines have been shifted $\pm QN$ from the origin, so that they have the same abscissa as the dashed lines. With these shifts the level repulsion occurs at $p_1 = 0$, where the $\Sigma = 0$ energy bands are degenerate with $E_+ = E_- = \sin(QN/2)$.

lower all the energies in the Fermi sea (see dashed blue line in figure 1). This *decreases* the baryon contribution to the free energy of the system with respect to the $\Sigma = 0$ case. In contrast, if we choose $Q = 0$ then S_I is a simple mass term that makes

$$\sinh E_\pm = \sqrt{\Sigma^2 + \sin^2(p_1/2)}, \tag{2.45}$$

and *increases* the energy of the Fermi sea (see dotted green line in figure 1). As a result, if we denote the contribution of the baryons to the free energy by $\mathcal{E}_B(\Sigma, Q)$ then

$$\mathcal{E}_B(\Sigma, p_F/N) < \mathcal{E}_B(0,0) < \mathcal{E}_B(\Sigma, 0), \tag{2.46}$$

and so, for $\mu > 0$, the Fermi sea energetically prefers that the condensates in eqs. (2.18) carry a nonzero momentum Q.

In the discussion above we have ignored many details. Firstly, we addressed only $d = 1$, where both the Fermi sphere and the gap occur at single points that can always be made to coincide. For $d > 1$, the Fermi sphere is a curved surface, and it is not assured that one can find a wave $\vec{Q}$ that will change the energy bands such that all the energies in the Fermi sea are pushed down. Indeed, it is known in condensed matter physics that similar inhomogeneous instabilities take place for $d > 1$ only for sufficiently strong interactions [2, 3]. Secondly, we discussed only the contribution of the Fermi sea to the free energy. The remaining contributions are the anti-baryons energy (coming in the form of the negative energy bands $\bar{E}_\pm$ of the Dirac sea) and the meson self-energy coming from

JHEP03(2007)016

$S_{\rm Meson}$. In fact, as we find in the next sections, both these contributions depend on Q, and can prefer $Q = 0$ for all values of $\mu \geq 0$. Thirdly, Σ may also depend on Q, while in the discussion above we have treated it as being fixed.

Finally, note that our discussion relies on the level repulsion presented in figure 1, where we choose $\Sigma = 0.1$. Since S_I also gives mass to the baryons (see eq. (2.45)), this means that we have, so far, had in mind small baryon masses. It is a priori unclear whether the chiral wave instability occurs for large values of Σ and very massive baryons, but what is clear is that if the energy bands of the baryons in the crystalline phase look qualitatively like what we present in figure 1, then it is natural to expect this instability when $NQ \simeq p_F$. More precisely, by comparing the solid black lines and the dashed blue lines in figure 1, we see that what allows the crystalline phase (that has nonzero Σ and Q) to compete with the massless phase (that has $\Sigma = 0$) is the fact that it has gapless excitations.

To study the effects of the issues we mention above on the viability of the chiral density waves, we develop a mean-field analysis for inhomogeneous vacua in the next section.

3. Mean-field theory

We start from eq. (2.12) and introduce auxiliary fields for the expectation values of $m_n, (m_n)^2, \ldots, (m_n)^N$ by writing [20]

$$\begin{aligned} \exp\left[N\sum_{n\nu} F_N(m_n m_{n+\hat{\nu}})\right] &= \exp\left[N\sum_{q=1}^{N}\sum_{n\nu} a_q m_n^q m_{n+\hat{\nu}}^q\right] \\ &= \int DV \exp\left[N\sum_{q=1}^{N}\sum_{n\nu} a_q V_{q,n} V_{q,n+\hat{\nu}}\right]\delta(V_{q,n} - m_n^q) \\ &= \int DV\,Dh \exp\left[N\sum_{q=1}^{N}\sum_{n\nu} a_q V_{q,n} V_{q,n+\hat{\nu}} - N h_{q,n}\,(V_{q,n} - m_n^q)\right]. \end{aligned} \tag{3.1}$$

Here $\int dV \equiv \prod_q \int_{-\infty}^{\infty} dV_R^{(q)} \int_{-\infty}^{\infty} dV_I^{(q)}$, and $V_{R,I}^{(q)}$ are the real and imaginary parts of V_q, while $\int dh \equiv \prod_q \int_{-i\infty}^{i\infty} dh_q^{(1)} \int_{-i\infty}^{i\infty} dh_q^{(2)}$. Also, $h_q V_q$ means $h_q^{(1)} V_R^{(q)} + h_q^{(2)} V_I^{(q)}$, and similarly for $h_q (m)^q$. Proceeding from eq. (3.1), the action for the scalar fields V and h becomes

$$S_{\rm eff}(V,h) = N\sum_{q=1}^{N} a_q \sum_{n\nu} V_{q,n} V_{q,n+\hat{\nu}} - N\sum_{n,q} h_{q,n} V_{q,n} + S_0, \tag{3.2}$$

$$\exp(S_0) = \int D\bar{b}\, Db\, Dm\, \exp\left\{\bar{b}\cdot\left[2^{N-1} d_N m^{-N}\mathbf{1} + D\right]\cdot b + N\sum_{q,n} h_{q,n} m_n^q\right\}. \tag{3.3}$$

The starting point of Mean field theory is to write the path integral for the action in eq. (3.2) as

$$Z(\lambda) \equiv \int Dh\, DV\, e^{\frac{1}{\lambda} S_{\rm eff}} \tag{3.4}$$

and to approach the physical point, $\lambda = 1$, by expanding around $\lambda = 0$ [20]. Calculating $O(\lambda)$ corrections is, however, outside the scope of the work we present here, and we study only the $O(\lambda^0)$ level. In this case, the tree-level mean-field equations are

$$\frac{\partial S_{\text{eff}}}{\partial V_{q,n}} = 0, \qquad \text{and} \qquad \frac{\partial S_{\text{eff}}}{\partial h^{(1,2)}_{q,n}} = 0, \tag{3.5}$$

which give

$$h^{(1)}_{q,n} = a_q \sum_{\nu=\pm 0}^{\pm d} V_{q,n+\hat{\nu}}, \tag{3.6}$$

$$h^{(2)}_{q,n} = i a_q \sum_{\nu=\pm 0}^{\pm d} V_{q,n+\hat{\nu}}, \tag{3.7}$$

$$V_{q,n} = \langle m^q_n \rangle. \tag{3.8}$$

Here the average $\langle , \rangle$ in eq. (3.8) is with respect to the path integral in eq. (3.3).

Equations (3.6)–(3.7) tell us to try an ansatz with $h^{(2)} = ih^{(1)} \equiv ih$, in which case the hV and hm terms in eq. (3.2) and eq. (3.3) have the meaning of a simple complex multiplication. Restricting to this type of ansatze we use

$$\oint \frac{dm}{2\pi i m} m^k = \delta_{k,0}, \tag{3.9}$$

to perform the $\int Dm$ integral in eq. (3.3), and we find (for $N = 3$)

$$\oint \frac{dm}{2\pi i m} \exp\left[3\left(h_1 m + h_2 m^2 + h_3 m^3\right) + \frac{8}{9} m^{-3} \bar{b} b\right] = \exp\left[4\left(h_1^3 + 2h_1 h_2 + \frac{2}{3} h_3\right) \bar{b} b\right]. \tag{3.10}$$

This turns $Z(1)$ of eq. (3.4) to

$$Z = \int DV\, Dh\, D\bar{b}\, Db\, \exp S_{\text{eff}}, \tag{3.11}$$

$$S_{\text{eff}} = N \sum_{q=1}^{N} a_q \sum_{n\nu} V_{q,n} V_{q,n+\hat{\nu}} - N \sum_{n,q} h_{q,n} V_{q,n} + \sum_{n,m} \bar{b}_n \left[\Sigma_n \mathbf{1} + D\right]_{nm} b_m, \tag{3.12}$$

$$\Sigma_n = 4\left(h^3_{1,n} + 2h_{1,n} h_{2,n} + \frac{2}{3} h_{3,n}\right). \tag{3.13}$$

The next step is to *assume* an ansatz for the spatial behaviour of $V_{q,n}$ and $h_{q,n}$. Here we allow for the possibility of the broken translation invariance, and write

$$V_{q,n} = V_q \exp\left(+iq\,\epsilon_n \vec{Q}\,\vec{n}\right), \qquad h_{q,n} = h_q \exp\left(-iq\,\epsilon_n \vec{Q}\,\vec{n}\right), \tag{3.14}$$

with real h_q and V_q. This ansatz breaks the symmetry of spatial translations as well as the $\mathrm{U}(1)_\epsilon$ chiral rotations

$$V_{q,n} \to V'_{q,n} = e^{i\,\epsilon_n\, q\,\theta}\, V_{q,n}, \qquad h_{q,n} \to h'_{q,n} = e^{-i\,\epsilon_n\, q\,\theta}\, h_{q,n}, \tag{3.15}$$

and, as we discuss in section 2.2, implies a helical structure for the chiral condensate.

A substitution of eq. (3.14) in eq. (3.6) gives

$$h_q = 2(d+1)a_q V_q \gamma_q(Q), \tag{3.16}$$

where

$$\gamma_q(Q) \equiv \frac{1}{d+1}\left[1 + \sum_{i=1}^{d} \cos\left(qQ_i\right)\right], \tag{3.17}$$

and a subsequent substitution of that into eq. (3.8), with a use of

$$\frac{\partial \Sigma_n}{\partial h_{nq}} = 4 \times \begin{cases} 3h_{1,n}^2 + 2h_{2,n} & q = 1 \\ 2h_{1,n} & q = 2 \\ \frac{2}{3} & q = 3 \end{cases}, \tag{3.18}$$

gives the final form of the mean-field equations

$$h_1 = \frac{9}{2}\frac{a_1\gamma_1}{a_3\gamma_3}\left(h_1^2 + \frac{2a_2\gamma_2}{a_3\gamma_3}h_1h_3\right)h_3, \tag{3.19}$$

$$h_2 = \frac{3a_2\gamma_2}{a_3\gamma_3}\, h_1h_3, \tag{3.20}$$

$$h_3 = \frac{16(d+1)a_3\gamma_3}{9} \times A(h_q, Q; \mu). \tag{3.21}$$

Also, $a_{1,2,3} = \frac{1}{4}, \frac{3}{64}, -\frac{15}{256}$, are the coefficients in F_3 (see eq. (2.5)), and $\gamma_{1,2,3}$ are given in eq. (3.17) (Here, for brevity, we write γ_q to denote $\gamma_q(Q)$). The function $A(h_q, Q; \mu)$ is defined as

$$A(h_q, Q; \mu) \equiv \langle \bar{b}_n b_n \rangle \cdot e^{-3i\vec{Q}\vec{n}\epsilon_n} = \frac{\partial \,\mathrm{tr}\, \log\left[\Sigma_n \mathbf{1} + D\right]}{\partial\left(\Sigma_n e^{3i\vec{Q}\vec{n}}\right)}, \tag{3.22}$$

and the derivative here is evaluated at

$$\Sigma_n = \Sigma e^{-3i\vec{Q}\vec{n}}, \tag{3.23}$$

$$\Sigma = 4\left(h_1^3 + 2h_1h_2 + \frac{2}{3}h_3\right). \tag{3.24}$$

To determine which of the solutions of the mean-field equations is the true vacuum we calculate the mean-field free energy. Using eq. (3.16), the energy per number of sites N_s can be expressed in terms of the fields h_q alone, and we find

$$\mathcal{E} \equiv -S_{\mathrm{eff}}^{\mathrm{mean-field}}/N_s = \frac{3}{4}\sum_q \frac{h_q^2}{(d+1)a_q\gamma_q(Q)} + \mathcal{E}_{\mathrm{matter}}, \tag{3.25}$$

where the contribution of the b fields is

$$\mathcal{E}_{\mathrm{matter}} = -\frac{1}{N_s}\mathrm{tr}\, \log\left[\Sigma_n \mathbf{1} + D\right]. \tag{3.26}$$

We calculate $A(h_q, Q; \mu)$ and $\mathcal{E}_{\rm matter}$ in appendix A, where we also show that the right hand side of eq. (3.22) is indeed independent of the lattice site index n. The result for $\mathcal{E}_{\rm matter}$ is

$$\mathcal{E}_{\rm matter} = -\frac{1}{2}\sum_{b=\pm}\int\left(\frac{dp}{2\pi}\right)^d (E_b - 3\mu)\,\theta\,(E_b - 3\mu)\,, \tag{3.27}$$

where $\theta(x)$ is the step function. The momentum integrals are from $-\pi$ to π, and $E_\pm$, that replace $E^{(1),(2)}$ of eq. (2.31), are the band energies of the baryons. In this paper we focus on $d = 3$ and $\vec{Q} = Q\hat{z}$, for which the dispersions are

$$\sinh^2 E_\pm = \sin^2(p_x/2) + \sin^2(p_y/2) + \left(\sqrt{\Sigma^2 + s_z^2} \pm |c_z|\right)^2, \tag{3.28}$$

$$s_z \equiv \sin(p_z/2)\cos 3Q/2, \tag{3.29}$$

$$c_z \equiv \cos(p_z/2)\sin 3Q/2. \tag{3.30}$$

(For the general dispersions with $\vec{Q} = (Q_x, Q_y, Q_z)$ see appendix A). Σ is related to the expectation values $V_q = \langle m_n^q \rangle$ through Eqs (3.6)–(3.8) and for $Q = 0$ it is the spectral gap that defines the baryon mass m_B (see eq. (3.28))

$$\sinh m_B = \Sigma. \tag{3.31}$$

From here on we refer to energy bands of eq. (3.28) with $\Sigma > 0$ as massive bands, and to energy bands with $\Sigma = 0$ as massless bands.

In figure 2 we plot $E_\pm$ for $\vec{p} = (0, 0, p_z)$. In the upper panel we choose $m_B = 3$ (or $\Sigma \sim 10$), which is close to the value that solves the mean-field equations in $d = 3$ and $\mu = 0$ (see next section). We present the cases of $Q = 0$, where $E_\pm$ are degenerate, and $Q = \pi/3$, where this degeneracy is removed. In the lower panel we show the case of $m_B = 0$ (or $\Sigma = 0$), where $E_\pm$ are again degenerate and also independent of Q.

Finally, to make a connection with the discussion in section 2.2 leading to eq. (2.46), we write eq. (3.27) as

$$\mathcal{E}_{\rm matter} = -|\mathcal{E}_{\bar{B}}| + \mathcal{E}_B - 3\mu\, n_B, \tag{3.32}$$

where the anti-baryon and baryon energies, $-|\mathcal{E}_{\bar{B}}|$ and $\mathcal{E}_B$, are given by

$$-|\mathcal{E}_{\bar{B}}| = +3\mu - \frac{1}{2}\sum_{b=\pm}\int\left(\frac{dp}{2\pi}\right)^d E_b, \tag{3.33}$$

$$\mathcal{E}_B = \frac{1}{2}\sum_{b=\pm}\int\left(\frac{dp}{2\pi}\right)^d (E_b - 3\mu)\,\theta\,(3\mu - E_b)\,, \tag{3.34}$$

and the baryon number density n_B is

$$n_B = \frac{1}{2}\sum_{b=\pm}\int\left(\frac{dp}{2\pi}\right)^d \theta\,(3\mu - E_b)\,. \tag{3.35}$$

4. The Mean-field ground state

In this section we present the solutions for the mean-field equations eqs. (3.19)–(3.21), and their corresponding energy densities. To understand the results we then study a formal limit of eq. (2.12) where one takes $N \to 1$.

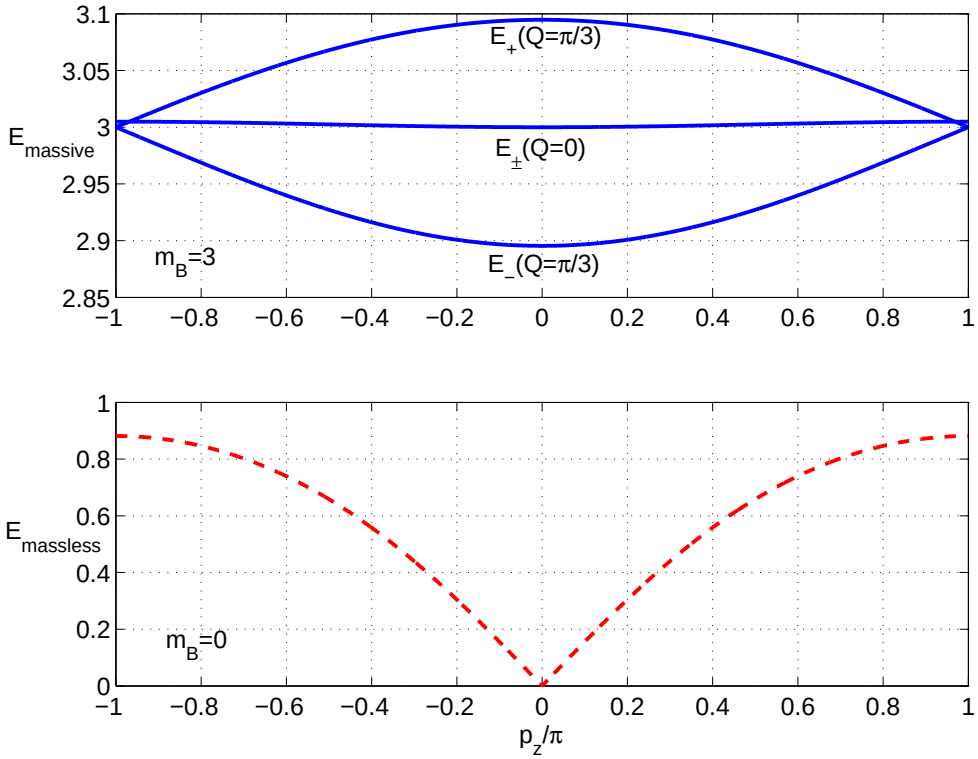

Figure 2: The energy bands $E_\pm$ of eq. (3.28) for $p = (0, 0, p_z)$. Upper panel: Massive bands with $m_B = 3$ and $Q = \pi/3$ (highest and lowest curves), and $Q = 0$ (middle curve). The bands $E_\pm(Q = 0)$ are degenerate and very flat, ranging between $E = 3$ and $E = \sqrt{\sinh^2(3) + \max\left(\sum_{i=1}^{3} \sin^2(p_i/2)\right)} \simeq 3.0147$. Lower panel: The massless band with $\Sigma = 0$.

4.1 Physical case : $N = 3$ and $d = 3$

We begin by describing the solution to the mean-field equation that leaves chiral symmetry intact in section 4.1.1, and proceed to discuss the chiral broken phase in section 4.1.2. Finally, in section 4.1.3 we discuss how the ground state evolves with increasing values of μ.

4.1.1 Solution I : Intact chiral symmetry

The first solution to the mean-field equations is obtained by taking $h_1 = h_2 = h_3 = 0$. This corresponds to a phase with intact chiral symmetry, $V_1 = V_2 = V_3 = 0$, and zero baryon mass $\Sigma = \sinh(m_B) = 0$. In this case the energy bands are trivially independent of Q (since $S_I^{\text{mean-field}} = 0$), and $E_\pm$ are degenerate

$$E_\pm = \sinh^{-1} \sqrt{\sum_{\nu=1}^{d} \sin^2(p_\nu/2)} \equiv E_{\text{massless}}. \tag{4.1}$$

The energy and baryon number densities of this solution are independent of Q as well, and

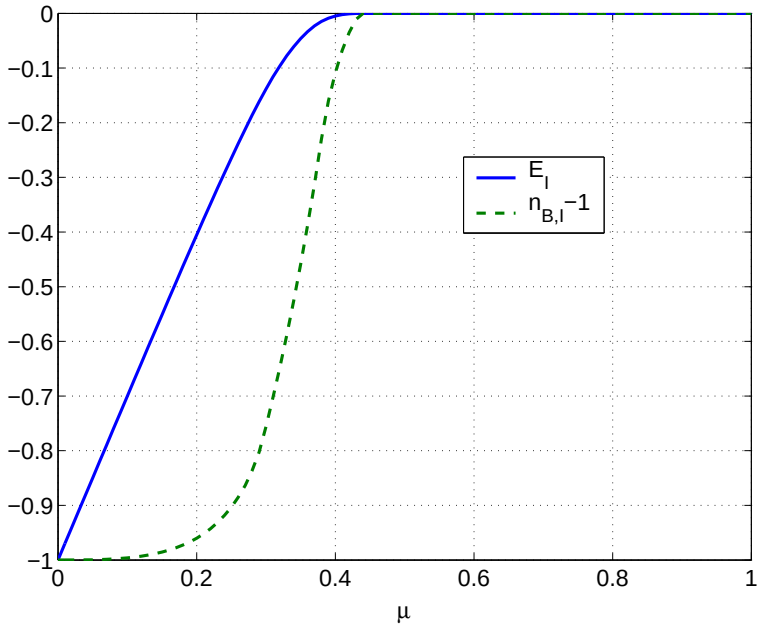

Figure 3: The energy density, $\mathcal{E}_I$, (solid line) and baryon number density, $n_{B,I}$, for the massless energy bands of solution type I, as a function of the chemical potential μ.

are given by

$$\mathcal{E}_I = -\int \left(\frac{dp}{2\pi}\right)^3 (E_{\text{massless}} - 3\mu)\,\theta\,(E_{\text{massless}} - 3\mu)\,, \tag{4.2}$$

$$n_{B,I} = \int \left(\frac{dp}{2\pi}\right)^3 \theta\,(3\mu - E_{\text{massless}})\,. \tag{4.3}$$

In figure 3 we plot $\mathcal{E}_I$ as a function of μ, where one can see that for $\mu = 0$, we get $\mathcal{E}_I \simeq -1$. As we increase μ, the energy density increases, and saturates when $\mu = \mu_s \simeq 0.439$, where it reaches zero. Looking at the form of E_{massless} from figure 2, we can understand why. The maximum energy to which E_{massless} of eq. (4.1) can reach is $\sinh^{-1}\sqrt{\max\sum_{i=1}^{3}\sin^2(p_i/2)} \simeq 1.317$. This means that when $\mu > \mu_s$, where the baryon chemical potential 3μ is already larger than $3 \times 0.439 \simeq 1.317$, the band E_{massless} is already saturated. This saturation can be seen also in the plot of the baryon number density, $n_{B,I}$ which reaches $n_{B,I} = 1$ at μ_s.

4.1.2 Solution II : Spontaneously broken chiral symmetry

In this case $h_{1,2,3}$ are nonzero, and we divide eq. (3.19) with h_1 to obtain

$$h_1 = \frac{2}{9}\frac{a_3\gamma_3}{a_1\gamma_1}\frac{1}{h_3} - \frac{2a_2\gamma_2}{a_3\gamma_3}h_3. \tag{4.4}$$

Substituting this in eq. (3.20) and eq. (3.24) we get Σ as a function of h_3, which we then substitute into eq. (3.21) and obtain a single equation for h_3, that we solve for all values of Q and μ.

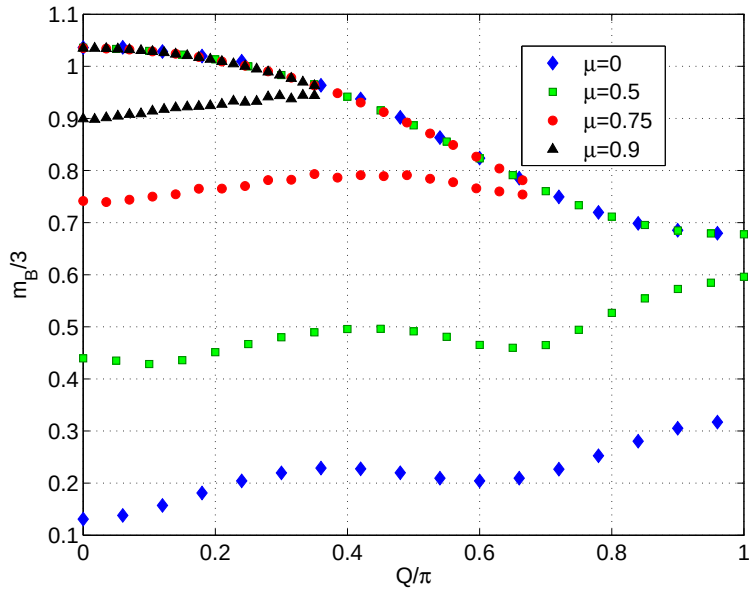

Figure 4: The values of $\frac{1}{3}m_B(Q;\mu)$ that solve the mean-field equations. Note the two branches of the solution, and that one of them (branch no.1, ending at $Q = 0$, and $m_B/3 = 1.0347$) hardly changes with μ. We find that this branch has a lower energy and therefore corresponds to the ground state (see text).

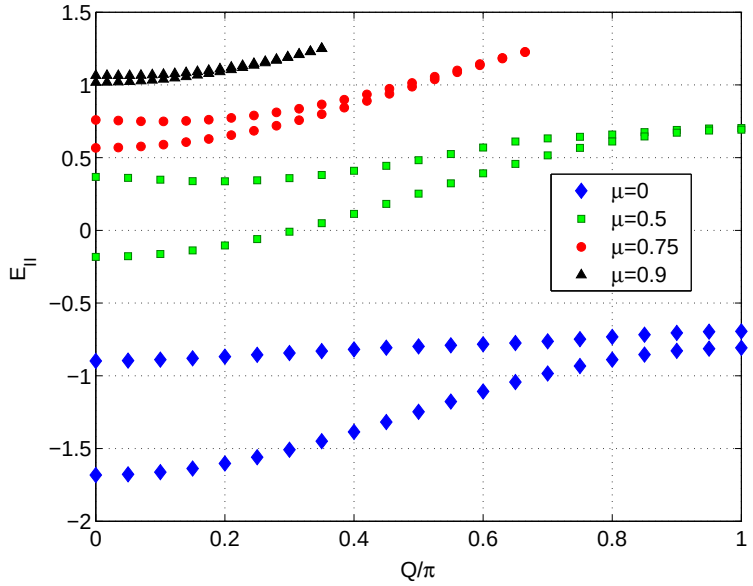

Figure 5: The energy density $\mathcal{E}_{\rm II}$ as a function of Q and μ for solution II. The lower branch (branch no.1) for each μ is the one that ends at $Q = 0$ and $m_B/3 = 1.0347$ (see figure 4).

The results are presented in figure 4 where we show $m_B \equiv \sinh^{-1}(\Sigma)$ as a function of Q, for $\mu = 0, 0.5, 0.75, 0.9$. In figure 5 we show the energy densities of these solutions. There are two branches in both figures that correspond to two solutions of type II that we find. From figures 4– 5, we see that at $\mu = 0$ the minima of both branches (referred to as

branches no. 1-2 below) is at $Q = 0$ and have

$$m_B^{(1)}/3 \simeq 1.0347, \quad \text{with} \quad \mathcal{E}_{\rm II}^{(1)} \simeq -1.6826, \tag{4.5}$$

$$m_B^{(2)}/3 \simeq 0.1309, \quad \text{with} \quad \mathcal{E}_{\rm II}^{(2)} \simeq -0.8981. \tag{4.6}$$

Consequently, the ground state of Solution II at $\mu = 0$ is given by the minimum of branch no. 1 (eq. (4.5)).

To see whether the chiral wave instability takes place, we consider figure 5 and find that the minima of $\mathcal{E}_{\rm II}$ is at $Q = 0$ for all values of μ. This is not in contradiction with the discussion of section 2.2 because, there, we only showed that the baryon contribution to the free energy, $\mathcal{E}_B(\Sigma, Q)$, has a minimum at $Q \neq 0$. What we see here is that the remaining contributions to $\mathcal{E}$ offset this minimum and lead to a ground state with $Q = 0$.

It is important to note that even if the minimum of $\mathcal{E}_B$ was deeper, such that $\mathcal{E}_{\rm II}$ itself had a minimum at $Q \neq 0$, it is still unlikely that the chiral density wave would become the ground state. To understand why, recall that in section 2.2 we showed that what allows the crystalline phase to compete with the $\Sigma = 0$ phase of Solution I are the gapless excitations in the baryon spectrum. From eq. (3.28) we see that the momentum of these excitations is given by

$$\vec{p} = (0, 0, p_z), \tag{4.7}$$

$$\sin^2 p_z/2 = \sin^2(NQ/2) - \Sigma^2, \tag{4.8}$$

which has a solution only if

$$\Sigma \leq 1. \tag{4.9}$$

Unfortunately, with the baryon mass of our ground state (4.5) we have $\Sigma = \sinh m_B \sim 11$. This prohibits gapless excitations, and makes the appearance of the chiral waves improbable.[3]

4.1.3 Evolution of mean-field ground state as a function of μ

Here we discuss the way the ground state evolves with increasing chemical potential μ. Given the conclusions of the previous sections, we restrict to states with $Q = 0$ only.

At $\mu = 0$, solution of type I has $\mathcal{E}_I \simeq -1$, while the solution of type II that has the lowest energy is given in eq. (4.5). Comparing $\mathcal{E}_I$ and the energy in eq. (4.5) we see that the latter is the ground state of the system, and so, the baryon mass is $m_B/3 \simeq 1.0347$. The condensates V_q (eq. (2.18)) that we find for this ground state are

$$\langle \frac{\bar{\chi}\chi}{3} \rangle = V_1 \simeq 0.67685, \tag{4.10}$$

$$\langle \left(\frac{\bar{\chi}\chi}{3}\right)^2 \rangle = V_2 \simeq 0.31947, \tag{4.11}$$

$$\langle \left(\frac{\bar{\chi}\chi}{3}\right)^3 \rangle = V_3 \simeq 0.07872. \tag{4.12}$$

[3]The true relevant value of Σ that should tested against eq. (4.9) is $\Sigma(Q;\mu) \equiv \sinh m_B(Q;\mu)$, but from figure 4 we see that $\Sigma(Q;\mu) \geq \Sigma(\pi;0) \simeq 4$, for which eq. (4.9) is still not satisfied.

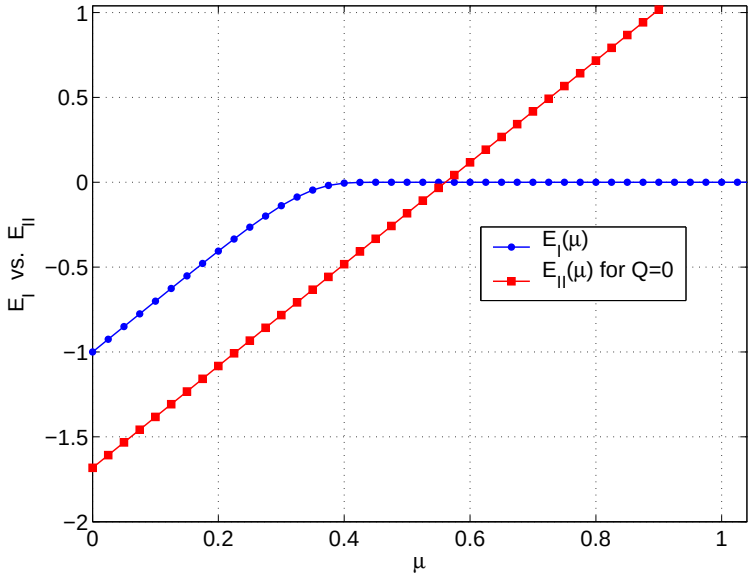

Figure 6: The energy densities $\mathcal{E}_I$ and $\mathcal{E}_{\rm II}$ as a function of μ.

Comparing these results to the literature, we see that our mass is $0.22\% - 0.54\%$ lower than other tree level results (see, for example, the summary in [22]), and that our condensates are close to the analytical and numerical results of [15, 17, 21, 23, 22] (discrepancies are on the level of $2\% - 5\%$).

When μ increases, the energy densities of both type of solutions grow. As explained in section 4.1.1, the energy of solution I stops increasing at μ_s where it reaches $\mathcal{E}_I = 0$. Nothing special happens to solution II at this point, and its energy is still negative and continues to grow monotonically. In figure 6 we replot $\mathcal{E}_I(\mu)$ of figure 3 together with the ground state value of $\mathcal{E}_{\rm II}(\mu)$ (i.e. for given μ, we extract the minima of the curves in figure 5).

From figure 6 we see that a transition occurs at $\mu = \mu_t$ where

$$\mathcal{E}_{\rm II}(\mu_t) = 0. \tag{4.13}$$

Substituting eq. (3.25) and eq. (3.16) in eq. (4.13) gives (for $Q = 0$)

$$3(d+1)\sum_{q=1}^{3} a_q\, V_q^2 = \int \left(\frac{dp}{2\pi}\right)^3 (E - 3\mu_t)\,\theta\,(E - 3\mu_t)\,. \tag{4.14}$$

From figure 4 we see that, for $Q = 0$, the mass m_B does not change as a function of μ up to $\mu \simeq m_B/3$, at which point solution II disappears. This reflects the fact that the condensates V_q are independent of μ as well, and allows us to use the $\mu = 0$ values of m_B and V_q in eq. (4.14). This is a consistent procedure provided that the resulting μ_t obeys $\mu_t < m_B/3$.

Indeed, solving eq. (4.14) for μ_t gives

$$\begin{aligned}\mu_t &= \left(\frac{1}{3}\int\left(\frac{dp}{2\pi}\right)^3 E(p)\right) - 4\left(a_1 V_1^2 + a_2 V_2^2 + a_3 V_3^2\right) \\ &\simeq 1.0367 - (0.45813 + 0.01914 - 0.001452) = 0.5609,\end{aligned} \tag{4.15}$$

which is lower than $m_B/3 \simeq 1.0347$. Consequently this means that the chiral symmetry of eq. (1.4) is restored in a first order transition at $\mu_t \simeq 0.5609$ that separates a low density phase characterised by the baryon mass of eq. (4.5) and the chiral condensates in eqs. (4.10)–(4.12), and a high density phase where this symmetry is intact and the baryons are massless.

Let us emphasise that the way chiral symmetry is restored here is largely influenced by lattice artifacts of the infinite coupling limit. In particular, we cannot observe the crystalline phase partly because the mass of the baryons in lattice units, m_B, is around ~ 3. This prevents the baryons spectrum from having gapless excitations, and makes their contribution to the free energy $\mathcal{E}_B(m_B, Q)$ higher compared to what it would be with $m_B = Q = 0$. This is in contrast to the 'continuum-like' scenario that we discussed in section 2.2, where m_B was small, and $\mathcal{E}_B(m_B, Q) < \mathcal{E}_B(0, 0)$. In the next section we study such a continuum-like case by taking a formal limit of $S_{\rm HKS}$, in which the mass of the b fields is significantly smaller than discussed above.

4.2 The formal limit of $N \to 1$

In this section we study a formal limit of eq. (2.12), where one takes $N = 1$ and $F_N(u) = u/4$. In this case eq. (2.12) cannot be obtained from an underlying lattice gauge theory, but nevertheless seems to be useful to understand, since it shows chiral restoration with less lattice artifacts. In their original preprint, the authors of [15] have considered this limit as an example for a case where the baryonic terms in eq. (2.12) are important at $\mu = 0$. Here we approach this limit at nonzero μ and seek for signs of a crystalline solution for the mean-field equations. We first do so for $d = 1$, where it is known that crystalline instabilities are robust [2, 3]. (The physical significance of the result in this case is, however, unclear since the continuous $\mathrm{U}(1)_\epsilon$ symmetry cannot break in $1 + 1$ dimensions.)

We begin the analysis by noting that for $N = 1$, eq. (2.12) depends only linearly on $m_n m_{n+\hat{\nu}}$. This allows us to take $h_2 = h_3 = V_2 = V_3 = 0$, and to call $h_1 = h, V_1 = V$. The mean-field equations become (we keep d general at this stage)

$$h = 2(d+1)a_1 V \gamma_1(Q), \tag{4.16}$$

$$V = A(h, Q; \mu), \tag{4.17}$$

and the free energy is now given by

$$\mathcal{E} = \frac{h^2}{4(d+1)a_1\gamma_1(Q)} + \mathcal{E}_{\rm matter}. \tag{4.18}$$

Both $A(h, Q; \mu)$ and $\mathcal{E}_{\rm matter}$ are still defined in eqs. (3.22), and (3.26), with the difference that the dependence of Σ_n on h_n is now

$$\Sigma_n = h_n = h e^{-i\epsilon_n Q\, n_1}. \tag{4.19}$$

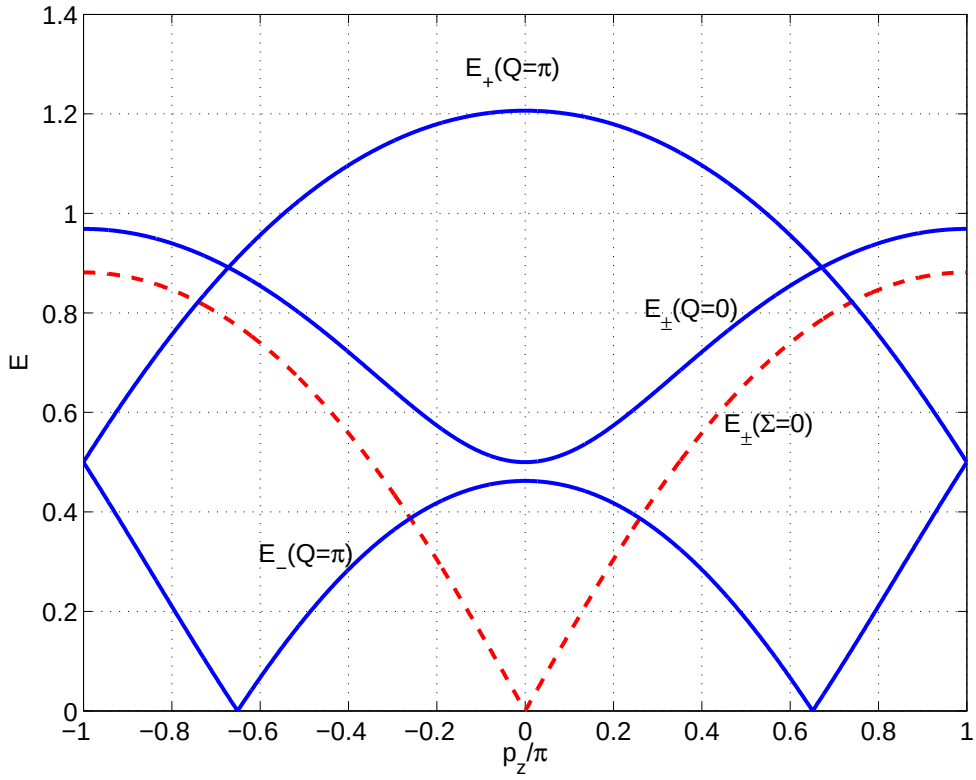

Figure 7: The energy bands $E_\pm$ of the baryons for $p = (0, 0, p_z)$. The dashed line is the gapless band with $m_B = 0$, and the solid lines are have $m_B = 0.5$, and $Q = 0, \pi$.

Again, it is easy to see that there are two type of solutions which are the analogues of the type I and II solutions in the SU(3) case. In figure 7 we present the energy bands for $m_B = \sinh^{-1}(\Sigma) = 0.5$, which is close to the value that solves the mean-field equations for $N = 1$ and $d = 1$. With this value of m_B the effect of the lattice coarseness is smaller compared to the $N = 3$ case : the massive and massless bands of solutions I and II overlap, and there exists momenta where the energy of solution II is zero.

As a result, a crystalline ground state is stable. In figure 8 we present the dependence of V and Q on μ. We also plot the following analytic expectation for $Q(\mu)$ that arises from our discussion in section 2.2 (adjusted to $N = 1$)

$$Q(\mu) = p_F(\mu) = 2 \sin^{-1}(\sinh \mu) \,. \tag{4.20}$$

It is clear that eq. (4.20) works well, especially for $\Sigma \ll 1$, which means that the mechanism described in section 2.2 is indeed the one generating the chiral density wave instability here.

When we move from $d = 1$ to $d = 2$ the crystalline phase disappears. We find that the reason is that the meson self energy described by the first term in eq. (4.18) prefers $Q = 0$, and 'wins' the instability generated in $\mathcal{E}_{\text{matter}}$. This effect comes from the function $\gamma_1(Q)$ in eq. (3.17), and can be considered as a lattice artifact as well, since in the continuum limit the lattice quantities Σ, μ, and Q vanish, and so $\gamma_1(Q) \to 1$. Indeed, in continuum

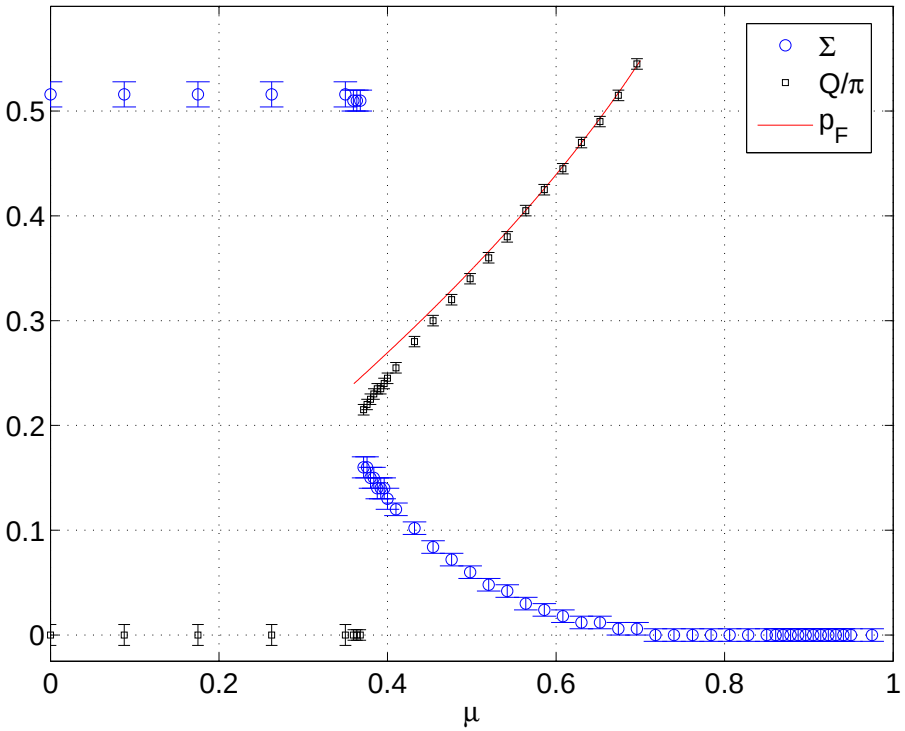

Figure 8: The values of V (circles), and Q/π (dots) that solve the mean-field equations (4.16)–(4.17) in $1+1$ dimensions. The red solid line denotes the analytic expression of eq. (4.20). Note that we present Q/π (black square symbols) only when $\Sigma > 0$, since otherwise $S_I^{\rm mean-field} = 0$, and Q is ill-defined.

treatments of the Nambu-Jona-Lasinio model such as [24], the contribution to the free energy that is the analog of the first term in eq. (4.18), does not depend on Q.

When we move to $d = 3$ it appears that even without the Q dependence in $\gamma_1(Q)$, the crystalline phase is unstable. This changes if one makes the meson self-interaction $F_1(u) = \frac{1}{4}u$ stronger by changing it to $F_1(u) = a_1 u$ with $a_1 > 1/4$.

5. Conclusions

Our aim in this paper was to see whether the phase diagram of strongly-coupled lattice QCD at zero temperature and nonzero density includes an incommensurate crystalline phase with chiral density waves. To do so we followed Hoek, Kawamoto, and Smit (HKS), and used the effective hadronic action, $S_{\rm HKS}$, that they derived in [15] for one-component staggered fermions. We formulated a mean-field theory for $S_{\rm HKS}$ which is novel in the following ways. Firstly, we do not neglect the terms in $S_{\rm HKS}$ that have four and six powers of the meson fields, and treat the baryon contribution in full. Secondly, our mean-field analysis is free of any undetermined parameters and we fix all vacuum expectation values by minimising the free-energy. Lastly, we do not assume a homogeneous ansatz, which is imperative in order to look for the crystalline phase. This leads us to introduce auxiliary

fields without the usual Hubbard-Stratonovich transformation, that can become ill-defined for inhomogeneous vacua.

Despite the fact that the generic structure of $S_{\rm HKS}$ can give rise to a crystal phase (see discussion in section 2.2), we find that this *does not* happen with our mean-field ansatz. This is partly due to lattice artifacts that come in the form of a large lattice baryon mass $m_B \sim 3$. The latter prohibits any possibility to have a gapless baryonic spectrum in the presence of the chiral density waves, which would allow the crystalline vacuum to compete with the massless homogeneous vacuum. To check this explanation, we take a formal limit of $S_{\rm HKS}$, where $m_B \simeq 0.5$, and indeed find that this lower mass can stabilise the crystal.

More precisely, when we study this formal limit in the $1+1$ system, we see a crystal structure at intermediate densities, with a wave vector given by the Fermi momentum of the system. However, this result is not robust; when we move to $2+1$ and $3+1$ dimensions we see that the crystalline instability is too weak to survive. The reasons for that include an additional lattice artifact, that does not go away when m_B decreases, and a too weak interaction between the fermions.

Our results stress that to get continuum physics from Monte-Carlo simulations at nonzero μ and low temperature, one will have to simulate on relatively fine lattices, with weak couplings. In particular, the baryon mass in lattice units, m_B, should be much smaller than its strong-coupling limit of $m_B \sim 3$. Only when this happens will the structure of the baryon energy bands be 'continuum-like'. For stronger couplings, the energy bands are *qualitatively* different than the continuum ones, and physical phenomena that are sensitive to their structure will also be *qualitatively* different than it is in the continuum. Chiral crystals is an good example for such a phenomenon, that simply goes away at strong couplings.

There are several ways in which one could extend this study. First, recall that we have focused on an ansatz that breaks translation invariance only in one direction. This direction was chosen to be along one of the lattice axes, but a further study can generalise this easily (we have already derived the free energy for a general $\vec{Q} = (Q_1, Q_2, Q_3)$) and check whether this makes the crystalline phase more robust. Second, as the authors in [4] point out, one can lower the energy of the crystalline phase by considering an ansatz which is a linear combination of waves, that will break translation invariance in all directions. Third, it will be useful (but also hard) to see how do the sub-leading terms in the strong-coupling expansion influence the results. These were obtained in [25] for the fermions we consider here, and give rise to more complicated interactions between the hadrons. Finally, it can be interesting to numerically study the possibility of chiral density waves in the Nambu-Jona-Lasinio model, where Monte-Carlo simulations are free from the sign-problem.

Acknowledgments

I thank J. Burkardt for help on using his numerical integration routines, J. Chalker and F. Essler for useful discussions, and Y. Shamir and B. Svetitsky for their remarks on this manuscript. I was supported by PPARC.

A. The baryonic determinant

In this section we calculate the baryonic determinant eq. (3.26) and its variation $A(h_q, Q; \mu)$ of eq. (3.22). We begin by showing that A, which, for the general SU(N) case, is defined by

$$A(h_q, Q; \mu) \equiv \langle \bar{b}_n b_n \rangle \, e^{-Ni\vec{Q}\vec{n}\,\epsilon_n}, \tag{A.1}$$

$$\langle \bar{b}_n b_n \rangle = \frac{\int D\bar{b}Db \; e^{S_0} \; \bar{b}_n b_n}{\int D\bar{b}Db \; e^{S_0}} \tag{A.2}$$

$$S_0 = \sum_{n,m} \bar{b}_n \left[\Sigma_n \mathbf{1} + D_{nm} \right] b_m, \tag{A.3}$$

is independent of the lattice site index n. To see this we use the symmetries of the action S_0

$$S_0 \equiv \bar{b}\, K\, b = \sum_n \bar{b}_n \, \Sigma e^{-iN\vec{Q}\vec{n}\epsilon_n} \, b_n + \frac{1}{2} \sum_{n\nu} \bar{b}_n \left(\eta_{n\nu} b_{n+\hat{\nu}} - \eta^{-1}_{n\nu} b_{n-\hat{\nu}} \right) \equiv S_\Sigma + S_{\rm kinetic}, \tag{A.4}$$

where $\epsilon_n = \pm$ is the parity of the site. In particular, $S_{\rm kinetic}$ is invariant under spatial translations

$$T_{\vec{R}} \quad : \quad n \to n + \vec{R} \tag{A.5}$$

and chiral symmetry

$$\mathrm{U}(1)_\epsilon \quad : \quad b_n \to e^{iN\theta\epsilon_n} b_n, \quad \bar{b}_n \to \bar{b}_n e^{iN\theta\epsilon_n}. \tag{A.6}$$

The term S_Σ is invariant under these symmetries only for the correlated transformation with $2\theta = \vec{Q} \cdot \vec{R}$. (More precisely, if R takes one from an even site to an odd site ($\epsilon_n = -\epsilon_{n+R}$) then an extra transformation of reflection around the origin is needed to keep S_Σ unchanged.)

Although S_0 is invariant under these correlated transformations, $\langle \bar{b}_n b_n \rangle$ is not, and transforms as follows

$$\text{For} \quad \epsilon_n = \epsilon_{n+\vec{R}} \quad : \quad \langle \bar{b}_n b_n \rangle \xrightarrow{\mathrm{T}_{\vec{\mathrm{R}}}} \langle \bar{b}_{n+\vec{R}} b_{n+\vec{R}} \rangle \xrightarrow{\mathrm{U}(1)_\epsilon} \langle \bar{b}_{n+\vec{R}} \, b_{n+\vec{R}} \rangle \, e^{-Ni\vec{Q}\vec{R}\epsilon_n} \tag{A.7}$$

$$\begin{aligned} \text{For} \quad \epsilon_n = -\epsilon_{n+\vec{R}} \quad : \quad & \langle \bar{b}_n b_n \rangle \xrightarrow{\mathrm{T}_{\vec{\mathrm{R}}}} \langle \bar{b}_{n+\vec{R}} b_{n+\vec{R}} \rangle \xrightarrow{\mathrm{U}(1)_\epsilon} \langle \bar{b}_{n+\vec{R}} \, b_{n+\vec{R}} \rangle \, e^{-Ni\vec{Q}\vec{R}\epsilon_n} \\ & \xrightarrow{\text{reflection}} \langle \bar{b}_{-(n+\vec{R})} \, b_{-(n+\vec{R})} \rangle \, e^{-Ni\vec{Q}\vec{R}\epsilon_n} = \langle \bar{b}_{-(n+\vec{R})} \, b_{-(n+\vec{R})} \rangle \, e^{+Ni\vec{Q}\vec{R}\epsilon_{-(n+\vec{R})}}. \end{aligned} \tag{A.8}$$

Putting $n = 0$ gives $\langle \bar{b}_0 b_0 \rangle = \langle \bar{b}_{\vec{R}} b_{\vec{R}} \rangle \, e^{-Ni\vec{Q}\vec{R}\epsilon_{\vec{R}}}$ for $\epsilon_{\vec{R}} = +1$ from eq. (A.7), and for $\epsilon_{\vec{R}} = -1$ from eq. (A.9). This proves that

$$\langle \bar{b}_n b_n \rangle \, e^{-Ni\vec{Q}\vec{n}\epsilon_n} = \text{independent of n}, \tag{A.9}$$

and therefore that[4]

$$A(h_q, Q; \mu) = \frac{1}{N_s} \frac{\partial \log \det \left[\Sigma \, e^{-Ni\vec{Q}\vec{n}\epsilon_n} \mathbf{1} + D \right]}{\partial \Sigma}. \tag{A.10}$$

[4]This is different from eq. (3.22) since here we evaluate the determinant for the helical ansatz, and then take the derivative with respect to Σ.

We now turn to calculate the determinant itself. It will be convenient to note that

$$\begin{aligned}\log\det K &\equiv \log\det\left[\Sigma e^{-iN\vec{Q}\vec{n}\epsilon_n}\mathbf{1}+D\right] \\ &= \log\det\left[\mathbf{1}+\Sigma^{-1}e^{Ni\vec{Q}\vec{n}\epsilon_n}D\right]+\sum_n\log\Sigma - Ni\sum_n\vec{Q}\vec{n}\epsilon_n,\end{aligned} \tag{A.11}$$

and to calculate $\det\tilde{K}\equiv\det\left[\mathbf{1}+\Sigma^{-1}e^{Ni\vec{Q}\vec{n}\epsilon_n}D\right]$ instead. (Note that the last term in eq. (A.12) drops out for a lattice with an even number of sites in each direction). To proceed, we use coordinates defined on a new lattice with spacing $a=2$, and write $n=2X+\rho$, with $\rho_{1,\ldots,d}=0$ or 1 and X taking values in the new lattice [19]. In these coordinates we use the following definitions

$$b_n \equiv b_\rho(X), \tag{A.12}$$

$$b_{n+\hat{\nu}} \equiv \sum_{\rho'}\left(\delta_{\rho',\rho+\hat{\nu}}b_{\rho'}(X)+\delta_{\rho',\rho-\hat{\nu}}b_{\rho'}(X+\hat{\nu})\right), \tag{A.13}$$

$$b_{n-\hat{\nu}} \equiv \sum_{\rho'}\left(\delta_{\rho',\rho-\hat{\nu}}b_{\rho'}(X)+\delta_{\rho',\rho+\hat{\nu}}b_{\rho'}(X-\hat{\nu})\right). \tag{A.14}$$

Moving to momentum space with

$$b_\rho(X) = \sqrt{\frac{2^d}{N_s}}\sum_p e^{i\left(pX+\epsilon_\rho\vec{Q}(2\vec{X}+\vec{\rho})/2\right)}b_\rho(p), \tag{A.15}$$

$$\bar{b}_\rho(X) = \sqrt{\frac{2^d}{N_s}}\sum_p e^{-i\left(pX+\epsilon_\rho\vec{Q}(2\vec{X}+\vec{\rho})/2\right)}\bar{b}_\rho(p), \tag{A.16}$$

we get

$$\tilde{S}_0 \equiv \bar{b}\,\tilde{K}\,b = \sum_{\substack{\rho,\rho'\\ p}}\bar{b}_\rho(p)\tilde{K}_{\rho\rho'}(p)b_\rho(p), \tag{A.17}$$

$$\tilde{K}_{\rho\rho'}(p) = \delta_{\rho\rho'}+\Sigma^{-1}\sum_\nu\left(\eta_\nu e^{ip'\nu/2}-\eta_\nu^{-1}e^{-ip'\nu/2}\right)\left(\delta_{\rho+\hat{\nu},\rho'}+\delta_{\rho-\hat{\nu},\rho'}\right)\mathrm{e}^{ip(\rho-\rho')/2}, \tag{A.18}$$

$$p' = p - NQ\epsilon_\rho, \tag{A.19}$$

where we used $\epsilon_\rho=-\epsilon_{\rho'}$. eq. (A.18) can be brought to the form

$$\tilde{K}(p) = \mathbf{1}+i\Sigma^{-1}\sum_{\nu=0}^{d}\Gamma_\nu(p)\,\sin\left(p_\nu/2-iN\mu\delta_{\nu,0}+NQ_\nu\hat{\epsilon}/2\right) \tag{A.20}$$

$$\begin{aligned}&= \mathbf{1}+i\Sigma^{-1}\left[\Gamma_0(\omega)\sin\left(\omega/2-iN\mu\right)\right. \\ &\quad\left.+\sum_{\nu=1}^{d}\Gamma_\nu(p)\,\sin(p_\nu/2)\cos(NQ_\nu/2)+\Gamma_\nu(p)\,\hat{\epsilon}\,\cos(p_\nu/2)\sin(NQ_\nu/2)\right]\end{aligned} \tag{A.21}$$

Here we defined

$$\left(\hat{\epsilon}\right)_{\rho\rho'} \equiv \epsilon_\rho\delta_{\rho\rho'}, \tag{A.22}$$

and also

$$(\Gamma_\nu)_{\rho\rho'} = \tilde{\eta}_\nu(\rho)\left(\delta_{\rho,\rho'+\hat{\nu}} + \delta_{\rho,\rho'-\hat{\nu}}\right) e^{ip(\rho-\rho')/2}, \tag{A.23}$$

where $\tilde{\eta}_\nu = \eta_\nu$ for $\nu \in [1,d]$ and $\tilde{\eta}_0 = 1$. The matrices Γ_ν obey

$$\{\Gamma_\nu, \Gamma_\tau\} = 2\delta_{\nu\tau}\mathbf{1}, \qquad \{\Gamma_\nu, \hat{\epsilon}\} = \{\Gamma_\nu, \Gamma_{5\tau}\} = 0, \tag{A.24}$$

with

$$(\Gamma_{5\nu})_{\rho\rho'} = i\tilde{\eta}_\nu(\rho)\left(\delta_{\rho,\rho'+\hat{\nu}} - \delta_{\rho,\rho'-\hat{\nu}}\right) e^{ip(\rho-\rho')/2}, \tag{A.25}$$

that also obey

$$\{\Gamma_{5\nu}, \Gamma_{5\tau}\} = 2\delta_{\nu\tau}\mathbf{1}, \qquad \{\Gamma_{5\nu}, \hat{\epsilon}\} = 0. \tag{A.26}$$

Next we use the fact that $\det \hat{\epsilon}\,\tilde{K}(p)\,\hat{\epsilon}\,\tilde{K}(p) = \det \tilde{K}^2(p)$ and that $\{\Gamma_\nu(p), \hat{\epsilon}\} = 0$ to get

$$\left(\det \tilde{K}(p)\right)^2 = \det \hat{\epsilon}\,\tilde{K}(p)\,\hat{\epsilon} \times \det \tilde{K}(p) \equiv \det K_2(p), \tag{A.27}$$

with

$$K_2(p) = \left(\epsilon\,\tilde{K}(p)\,\hat{\epsilon}\right)\tilde{K}(p) = \left[\mathbf{1}\left(1 + \Sigma^{-2}\left(\sum_{\nu=0}^{d} s_\nu^2 - \sum_{\nu=1}^{d} c_\nu^2\right)\right) + 2\Sigma^{-2}\sum_{\substack{\mu\neq\nu \\ \mu\neq 0}} s_\nu c_\mu \Gamma_\nu \Gamma_\mu\,\hat{\epsilon}\right]. \tag{A.28}$$

Here we defined

$$s_0 = \sin\left(p_0/2 - iN\mu\right), \tag{A.29}$$

and for $\nu > 0$

$$s_\nu = \sin(p_\nu/2)\cos(NQ_\nu/2), \tag{A.30}$$

$$c_\nu = \cos(p_\nu/2)\sin(NQ_\nu/2). \tag{A.31}$$

To proceed we need to find a matrix that anti-commutes with $\Gamma_\nu\Gamma_\mu\hat{\epsilon}$ for all $\nu \neq \mu$. We can choose any of the matrices $M = \Gamma_{5\nu}$ (which also obey $M^2 = \mathbf{1}$) and we have

$$\left(\det \tilde{K}(p)\right)^4 = \left(\det K_2(p)\right)^2 = \det MK_2(p)M \times \det K_2(p) \equiv \det K_4(p), \tag{A.32}$$

with

$$K_4(p) = (MK_2M)\,K = \left[\mathbf{1}\cdot\left(1 + \Sigma^{-2}\left(\sum_{\nu=0}^{d} s_\nu^2 - \sum_{\nu=1}^{d} c_\nu^2\right)\right)^2 - 4\Sigma^{-4}C^2\right],$$

$$C = \sum_{\substack{\mu\neq\nu \\ \mu\neq 0}} s_\nu c_\mu \Gamma_\nu \Gamma_\mu\,\hat{\epsilon}. \tag{A.33}$$

Using the anti-commutation relations of Γ_ν we get $C^2 = -B\cdot\mathbf{1}$ with

$$B = s_0^2\sum_{\nu=1}^{d} c_\nu^2 + \sum_{\substack{\nu\neq\mu \\ \nu,\mu\geq 1}} \left(s_\nu c_\mu - c_\nu s_\mu\right)^2, \tag{A.34}$$

and defining $D(p) \equiv \det K_4(p)$ we obtain the following form

$$D(p) \cdot \Sigma^4 = \left(\sin^2(p_0/2 - iN\mu) + \epsilon_+^2(p)\right) \times \left(\sin^2(p_0/2 - iN\mu) + \epsilon_-^2(p)\right). \quad \text{(A.35)}$$

Here

$$\epsilon_\pm^2 = |\vec{s}|^2 \sin^2\phi + \left(\sqrt{\Sigma^2 + |\vec{s}|^2\cos^2\phi} \pm |\vec{c}|\right)^2, \quad \text{(A.36)}$$

$$s_i \equiv \sin(p_i/2)\cos(NQ_i/2), \quad \text{(A.37)}$$

$$c_i \equiv \cos(p_i/2)\sin(NQ_i/2), \quad \text{(A.38)}$$

$$\cos\phi \equiv \hat{c}\cdot\hat{s}. \quad \text{(A.39)}$$

Since $\det\tilde{K}(-p) = \det\tilde{K}^*(p)$ then $\det\tilde{K} \equiv \prod_p \det\tilde{K}(p)$ is real[5] and we can write $\det\tilde{K} = \left(\det\tilde{K}^4\right)^{1/4} = \left(\prod_p \det K_4(p)\right)^{1/4}$ or

$$\log\det\tilde{K} = \frac{1}{4}\sum_p \log(D(p))^{2^d} = \frac{N_s}{4}\int_{-\pi}^{+\pi}\left(\frac{dp}{2\pi}\right)^{d+1}\log D(p). \quad \text{(A.40)}$$

Dropping irrelevant constants, we get

$$\frac{1}{N_s}\log\det K = \frac{1}{4}\sum_{b=\pm}\int_{-\pi}^{+\pi}\left(\frac{d\vec{p}}{2\pi}\right)^d\int_{-\pi}^{\pi}\frac{dp_0}{2\pi}\log\left[\sin^2(p_0/2 - iN\mu) + \epsilon_b^2\right], \quad \text{(A.41)}$$

$$\frac{1}{N_s}\frac{\partial\log\det K}{\partial\Sigma} = \frac{\Sigma}{2}\sum_{b=\pm}\int_{-\pi}^{+\pi}\left(\frac{d\vec{p}}{2\pi}\right)^d\int_{-\pi}^{\pi}\frac{dp_0}{2\pi}\frac{\left(1 + b\frac{|\vec{c}|}{\sqrt{\Sigma^2+\vec{s}^2\cos^2\phi}}\right)}{\sin^2(p_0/2 - iN\mu) + \epsilon_b^2(p)}. \quad \text{(A.42)}$$

Performing the change of variables $z \equiv e^{ip_0 - 2N\mu}$ the integral in eq. (A.42) becomes a simple contour integral and using complex analysis one can show that

$$\int_{-\pi}^{\pi}\frac{dp_0}{2\pi}\frac{1}{\sin^2(p_0/2 - iN\mu) + \epsilon_b^2} = \frac{\theta(E_b(p) - N\mu)}{\sqrt{\epsilon_b^2(1+\epsilon_b^2)}}, \quad \text{(A.43)}$$

where $\sinh^2 E_b(p,s) = \epsilon_b^2(p)$. The integration in eq. (A.41) is carried out as follows (dropping an irrelevant constant of integration)

$$\begin{aligned}\int_{-\pi}^{\pi}\frac{dp_0}{2\pi}\log\left[\sin^2(p_0/2 - iN\mu) + \epsilon_b^2(p)\right] &= \int_{X_0}^{\epsilon_b} dX\int_{-\pi}^{\pi}\frac{dp_0}{2\pi}\frac{1}{\sin^2(p_0/2 - iN\mu) + X} \\ &= 2\left[E_b(p) - N\mu\right]\theta(E_b(p) - N\mu). \quad \text{(A.44)}\end{aligned}$$

[5]This can be proved as follows. We have $\tilde{K}(p,Q) = \tilde{K}^*(-p,-Q)$, but also $\det\tilde{K}(p,Q) = \det\Gamma_{5\mu}\hat{\epsilon}\tilde{K}(p,Q)\hat{\epsilon}\Gamma_{5\mu} = \det\tilde{K}(p,-Q)$. This means that $\det\tilde{K}(p,Q)\det\tilde{K}(-p,Q) = \det\tilde{K}(p,Q)\det\tilde{K}^*(p,-Q) = \det\tilde{K}(p,Q)\det\tilde{K}^*(p,Q) = |\det\tilde{K}(p,Q)|^2$ is real.

JHEP03(2007)016

The final result is then

$$\frac{1}{N_s}\frac{\partial \log\det K}{\partial \Sigma} = \frac{\Sigma}{2}\sum_{b=\pm}\int\left(\frac{dp}{2\pi}\right)^d \frac{\left(1+b\frac{|\vec{c}|}{\sqrt{\Sigma^2+|\vec{s}|^2\cos^2\phi}}\right)}{\sqrt{\epsilon_b^2(1+\epsilon_b^2)}}\,\theta\left(E_b(p)-N\mu\right) \quad \text{(A.45)}$$

$$\frac{1}{N_s}\log\det K = \frac{1}{2}\sum_{b=\pm}\int\left(\frac{dp}{2\pi}\right)^d \left(E_b(p)-N\mu\right)\theta\left(E_b(p)-N\mu\right). \quad \text{(A.46)}$$

which we evaluate numerically. In particular, in the case of $d = 3$, we present results for $\vec{Q}||\hat{z}$, in which case

$$\epsilon_\pm^2 = |\vec{s}_\perp|^2 + \left(\sqrt{\Sigma^2+\vec{s}_z^2}\pm|c|\right)^2, \quad \text{(A.47)}$$

$$s_z = \sin(p_z/2)\cos(NQ/2), \quad \text{(A.48)}$$

$$c = \cos(p_z/2)\sin(NQ/2), \quad \text{(A.49)}$$

$$|\vec{s}_\perp|^2 = \sin^2 p_x/2 + \sin^2 p_y/2. \quad \text{(A.50)}$$

Since the transverse directions appear very simply here, we define the density of states $D(s)ds = \left(\frac{dp}{2\pi}\right)^{d-1}\delta\left(\sum_{\nu=x,y}\sin^2(p_\nu/2)-s\right)$ for the transverse momenta. One can show that $D(s) = \frac{2}{\pi^2}K(s(2-s))$ where $K(x)$ is the complete elliptic integral of the first kind (for example see [26]).

References

[1] D.V. Deryagin, D.Y. Grigoriev and V.A. Rubakov, *Standing wave ground state in high density, zero temperature QCD at large-$N(c)$*, *Int. J. Mod. Phys.* **A 7** (1992) 659.

[2] R.E. Peierls, *More surprises in theoretical physics*, Princeton University Press (1991).

[3] A. W. Overhauser, *Spin density waves in an electron gas*, *Phys. Rev.* **128** (1962) 1437.

[4] E. Shuster and D.T. Son, *On finite-density QCD at large-$N(c)$*, *Nucl. Phys.* **B 573** (2000) 434 [hep-ph/9905448].

[5] B.-Y. Park, M. Rho, A. Wirzba and I. Zahed, *Dense QCD: overhauser or BCS pairing?*, *Phys. Rev.* **D 62** (2000) 034015 [hep-ph/9910347].

[6] R. Rapp, E.V. Shuryak and I. Zahed, *A chiral crystal in cold QCD matter at intermediate densities?*, *Phys. Rev.* **D 63** (2001) 034008 [hep-ph/0008207].

[7] K. Rajagopal and E. Shuster, *On the applicability of weak-coupling results in high density QCD*, *Phys. Rev.* **D 62** (2000) 085007 [hep-ph/0004074].

[8] O. Schnetz, M. Thies and K. Urlichs, *The phase diagram of the massive Gross-Neveu model, revisited*, hep-th/0507120.

[9] P. de Forcrand and U. Wenger, *New baryon matter in the lattice Gross-Neveu model*, *PoS* **LAT2006** (2006) 152 [hep-lat/0610117].

JHEP03(2007)016

[10] V. Schon and M. Thies, *Emergence of Skyrme crystal in Gross-Neveu and 't Hooft models at finite density*, *Phys. Rev.* **D 62** (2000) 096002 [hep-th/0003195].

[11] L. Castillejo, P.S.J. Jones, A.D. Jackson, J.J.M. Verbaarschot and A. Jackson, *Dense skyrmion systems*, *Nucl. Phys.* **A 501** (1989) 801.

[12] N. Kawamoto, K. Miura, A. Ohnishi and T. Ohnuma, *Phase diagram at finite temperature and quark density in the strong coupling limit of lattice QCD for color* SU(3), *Phys. Rev.* **D 75** (2007) 014502 [hep-lat/0512023].

[13] M.P. Lombardo, *Lattice QCD at finite density: a primer*, *Prog. Theor. Phys. Suppl.* **153** (2004) 26 [hep-lat/0401021].

[14] M. Sadzikowski and W. Broniowski, *Non-uniform chiral phase in effective chiral quark models*, *Phys. Lett.* **B 488** (2000) 63 [hep-ph/0003282].

[15] J. Hoek, N. Kawamoto and J. Smit, *Baryons in the effective lagrangian of strongly coupled lattice QCD*, *Nucl. Phys.* **B 199** (1982) 495.

[16] P. Hasenfratz and F. Karsch, *Chemical potential on the lattice*, *Phys. Lett.* **B 125** (1983) 308.

[17] N. Kawamoto and J. Smit, *Effective lagrangian and dynamical symmetry breaking in strongly coupled lattice QCD*, *Nucl. Phys.* **B 192** (1981) 100.

[18] I. Bars, U(n) *integral for generating functional in lattice gauge theory*, *J. Math. Phys.* **21** (1980) 2678;
S. Samuel, U(n) *integrals,* $1/n$ *and the Dewit-'t Hooft anomalies*, *J. Math. Phys.* **21** (1980) 2695;
K.E. Eriksson, N. Svartholm and B.S. Skagerstam, *On invariant group integrals in lattice QCD*, *J. Math. Phys.* **22** (1981) 2276;
J. Hoek, SU(n) *one link integral by recursion*, *Phys. Lett.* **B 102** (1981) 129;
R.C. Brower and M. Nauenberg, *Group integration for lattice gauge theory at large-N and at small coupling*, *Nucl. Phys.* **B 180** (1981) 221;
S. I. Azakov and E. S. Aliev, *One link integral in the lattice QCD: strong coupling*, *Phys. Scripta* **38** (1988) 769.

[19] H. J. Rothe, *Lattice gauge theories: an introduction*, *World Sci. Lect. Notes Phys.* **74** (2005) 1.

[20] J. Zinn-Justin, *Quantum field theory and critical phenomena*, *Int. Ser. Monogr. Phys.* **113** (2002) 1.

[21] O. Martin, *Mesons and baryons at large-N and strong coupling*, *Phys. Lett.* **B 130** (1983) 411.

[22] P. de Forcrand and S. Kim, *The spectrum of lattice QCD with staggered fermions at strong coupling*, *Phys. Lett.* **B 645** (2007) 339 [hep-lat/0608012].

[23] Y. Nishida, *Phase structures of strong coupling lattice QCD with finite baryon and isospin density*, *Phys. Rev.* **D 69** (2004) 094501 [hep-ph/0312371].

[24] E. Nakano and T. Tatsumi, *Chiral symmetry and density wave in quark matter*, *Phys. Rev.* **D 71** (2005) 114006 [hep-ph/0411350].

[25] I. Ichinose, *Effective lagrangian of mesons and baryons in the strong coupling expansion of lattice QCD*, *Nucl. Phys.* **B 249** (1985) 715.

[26] J.E. Gubernatis, D.J. Scalapino, R.L. Sugar and W.D.R. Toussaint, *Two-dimensional spin-polarized fermion lattice gases*, *Phys. Rev.* **B 32** (1985) 103.

JHEP03(2007)016